nature materials

SUPPLEMENTARY INFORMATION

DOI: 10.1038/NMAT3049

Nanoparticles that Communicate *In Vivo* to Amplify Tumour Targeting

(Supplemental Materials and Methods)

Geoffrey von Maltzahn[1], Ji-Ho Park[2], Kevin Y. Lin[3], Neetu Singh[1], Christian Schwöppe[4], Rolf Mesters[4], Wolfgang E. Berdel[4], Erkki Ruoslahti[5,6], Michael J. Sailor[7,8], Sangeeta N. Bhatia[1,9].

[1]Harvard-MIT Division of Health Sciences and Technology, Massachusetts Institute of Technology, 77 Massachusetts Avenue, Cambridge, MA 02139 (USA); [2] Department of Bio and Brain Engineering, Korea Advanced Institute of Science and Technology, 291 Daehak-ro, Yuseong-gu, Daejeon 305-701, South Korea; [3] Department of Chemical Engineering, Massachusetts Institute of Technology, 77 Massachusetts Avenue, Cambridge, MA 02139 (USA);[4] Department of Medicine/Hematology and Oncology , University Hospital Muenster, D-48129 Muenster, Germany; [5]Vascular Mapping Laboratory, Center for Nanomedicine, Sanford-Burnham Medical Research Institute at UCSB, 3119 Biology II Bldg., University of California, Santa Barbara, CA 93106-9610; [6]Cancer Research Center, Sanford-Burnham Medical Research Institute, La Jolla, CA 92037; [7]Materials Science and Engineering Program, Department of Chemistry and Biochemistry, University of California, San Diego, 9500 Gilman, La Jolla, CA 92093 (USA); [8] Department of Chemistry and Biochemistry, University of California, San Diego, La Jolla, CA 92093-0358; [9] Electrical Engineering and Computer Science, MIT, David H. Koch Institute for Integrative Cancer Research, MIT, Department of Medicine, Brigham and Women's Hospital, Howard Hughes Medical Institute.

Materials and Methods:

PEG-NR Signalling Module Synthesis. PEG-NRs were synthesized as described previously(1). Briefly, highly stable, ~13 nm x 47 nm (Figure 2C) CTAB-coated gold nanorods with longitudinal plasmon resonance at 810 nm (Nanopartz, a division of Concurrent Analytical Inc., Salt Lake City, UT) coated in 250 μM 5 kDa methyl-PEG-thiol (Laysan Bio, U.S., Arab, AL). The solution of 5 kDa methyl-PEG-thiol and

DOI: 10.1038/NMAT3049

CTAB-coated gold nanorods was gently mixed at room temperature for 1 hr and dialyzed exhaustively against ultrapure water (18 MΩ cm^{-1}) via cellulose ester membrane dialysis (Spectrapor, Rancho Dominguez, CA) to drive PEG addition. Dialyzed samples were filtered through 100 kDa filters (Millipore, Billerica, MA) to remove excess polymer and stored at 4˚C.

tTF-RGD and tTF-NGR Signalling module expression, purification, and in vitro testing

The cDNAs coding for the tTF-containing amino acids 1 - 218 and the respective C - terminal peptide extension were amplified by polymerase chain reaction (PCR) using the primers:

5‘-CATGCCATGGGATCAGGCACTACAAATACTGTGGCAGCATATAAT-3‘(5‘-Primer)

5’-CGGGATCCTATTATGGAGAATCACCTCTTCCTCTGAATTCCCC-3’ (3‘-Primer) for tTF-RGD and

5’-CGGGATCCTATTATGCATGTGCTCTTCCGTTACCTCTGAATTCCCC-3’ (3‘-Primer) for tTF-NGR.

With the DNA-Ligation Kit (Novagen, Schwalbach am Taunus, Germany) the cDNA was cloned into the expression vector pET-30(+)a (Novagen) using the BamHI and NcoI sites of the vector. The vectors were introduced in competent *Escherichia coli* cells (BL21 DE3) according to the manufacturer’s protocol (Novagen). The bacteria were cultivated in Luria broth medium supplemented with kanamycin (30 µg/ml) at 37°C. When the bacteria cell suspensions reached an OD of ~ 0.6, over-expression of the fusion proteins was initiated by adding 1 mM IPTG (Novagen). After ~16 h, the cells were harvested and 5-7 ml lysis buffer (10 mM Tris-HCl, pH 7.5; 150 mM NaCl; 1 mM $MgCl_2$; 10 µg/ml aprotinin; 20 µl benzonase; 2 mg/ml lysozyme) per gram wet weight were added. The lysed cells were incubated for 90 minutes at room temperature (RT) and centrifuged at 12,000 g for 20 min at 4°C. The pellet was resuspended and homogenized by sonicating in washing buffer (10 mM Tris/HCl, pH 7.5; 1 mM EDTA, 3% Triton X-100). To solubilize the inclusion bodies, 2-4 ml guanidinium buffer (6 M GuCl, 0.5 M NaCl, 20 mM Tris/HCl, pH 7.5; 1 mM DTT) per gram wet weight was added. After incubation overnight at RT, the suspension was centrifuged at 10,000 g for 20 min at 4°C and the supernatant was filtered through a 0.22 µm filter.
The solubilized tTF fusion proteins were refolded and purified by using a multi-step HPLC-based purification process (HPLC unit: ÄKTA purifier 100 System, GE healthcare, Uppsala, Sweden). It consists of an immobilized metal-(copper-)affinity chromatography (IMAC; IMAC Sepharose 6 FF, GE healthcare). The histidine-tagged tTF fusion proteins bind to the immobilized copper ions so that the complete refolding (gradient from 6 M to 0 M urea buffer within 60 min) and washing processes are performed on the column, from which the tTF proteins are eluted by applying 300 mM imidazole. During the subsequent gel filtration the IMAC eluate is conditioned by a buffer exchanging step (20 mM Tris/HCl, pH 8; 20 % glycerol) using Sephadex G-25 (GE healthcare) in order to prepare for the following intermediate anion-exchange chromatography step (AIEX; Q Sepharose HP, GE healthcare; used buffers: 20 mM

Tris/HCl, pH 8; 20 % glycerol +/- 300 mM NaCl). The concluding polishing step again comprises a gel filtration using Sephadex G25 in order to remove any remaining trace impurities and to exchange the puffer to PBS. The final protein solutions (> 95% purity) are stored at -80°C.
Each sample produced was tested for purity (SDS-PAGE, Western Blot, endotoxins, HPLC) and activity (Factor-X coagulation test).

Factor-X activation by tTF Signalling modules
The ability of the tTF proteins to enhance the specific proteolytic activation of Factor (F) X by FVIIa was assessed as described by Ruf et al.(4). Briefly, to each well in a microtiter plate was added 20 µl of: (a) 50 nM recombinant FVIIa (Novo-Nordisc, Bagsværd, Denmark) in TBS-BSA; (b) 0.16 nM - 1.6 µM tTF/tTF-NGR in TBS containing 0.1 % bovine serum albumine (BSA); (c) 25 nM $CaCl_2$ and 500 µM phospholipids (phosphatidylcholine/phosphatidylserine, 70/30, MM; Sigma, München, Germany). After 10 min at RT, 20 µl of the substrate FX (Enzyme Research Laboratories, Swansea, UK) was added in a concentration of 5 µM. Aliquots were removed from the reaction mixture every minute and stopped in 100 nM EDTA. Spectrozyme FXa (American Diagnostica, Greenwich, CT, USA) was added and rates of FXa generation were monitored by the development of color at 405 nm with a microplate reader (Bio-Rad, Hercules, California, USA).

Fibrinogen deposition in heated tumours. Bovine fibrinogen (Sigma) and albumin (Sigma) were reacted with near-infrared fluorochromes (VT750-NHS or VT680-NHS) at a 2:1 fluorophore: protein molar ratio in PBS for ~2 hrs and dialyzed extensively at 4˚C against PBS to remove unreacted fluorophores. The product of the dialysis was passed through a 0.1µm filter, quantified using a BCA protein assay (Pierce), and assessed for fluorophore labelling via the absorption at the peak fluorphore absorbance (λ_{max}=750 and 680 nm, respectively, for VT750 and VT680). This reaction generated fibrinogen and albumin protein stocks carrying ~1 fluorophore/protein. To assess whether fibrinogen and albumin home to heated tumours, ~1 nanomole of both proteins (bearing distinct NIR-fluorophores) was injected intravenously into mice bearing bi-lateral MDA-MB-435 carcinoma tumours. Immediately following injection, one tumour on each mouse was externally heated using a temperature-controlled water bath set to between 41-53˚C for 20 min. At 24 hrs post-injection, mice were dissected and both tumours fluorescently imaged for the relative abundance of fibrinogen and albumin (LI-COR Odyssey Infrared Imaging System). To ensure that fluorophores did not optically or molecularly skew homing results, all fluorescent experiments were performed with equal numbers of mice allocated to VT750-fibrinogen/VT680-ablumin and VT680-fibrinogen/VT750-albumin administration at each temperature tested. Increases in protein tropism to heated tumours were analyzed by combining the fold increase in targeting observed for both fluorophore orientations (n=4 mice at each temperature tested).

Biodistribution and photothermal heating of passively-targeted nanorod Signalling modules in vivo. Nude mice were injected subcutaneously in the hind flank with ~$2x10^6$ MDA-MB-435 cells. After 2-3 weeks, animals were anaesthetized with isoflurane and injected through the tail vein with PEG-NRs in 0.15 M NaCl, 0.1 M Na Phosphate buffer, pH 7.2 (10 mg Au/kg, ~150ul bolus). Biodistribution was assessed by collecting

DOI: 10.1038/NMAT3049

organ samples for inductively-coupled plasma mass spectrometry (Thermo-Scientific Finnigan ELEMENT2). Samples were frozen, lyophilized, and dissolved in aqua regia, prepared by adding 100 ul of nitric acid + 300 ul of 37% hydrochloric acid for 72 hrs to dissolve gold particles. Then, samples were brought up into 10 mLs of 9.6 mL 2% HNO_3 and analyzed via ICP-MS against standards. Control saline and organ samples with exogenously added PEG-NRs were utilized to calibrate the linearity of this method. All photothermal heating of NRs was conducted at 72 hrs post administration (a time point after which they had completely cleared circulation) under the guidance of infrared thermography to continually illuminate the surface temperature of irradiated regions (FLIR Thermacam S60). A custom diode laser (RPMC Lasers Inc, 810nm, 30 W) was utilized to broadly irradiate the right flank of tumour-bearing mice at ~0.75 W/cm^2 and ~1 W/cm^2 to maintain desired peak tumour temperatures in NR-injected mice (~46°C for initial fibrinogen-homing experiments and integrated nanoparticle system implementation; 20 min exposure).

Quantifying tTF-RGD accumulation in tumours via fluorescence. Quantification of protein accumulation via fluorescence was based on previously described methods.(6-7) tTF-RGD was reacted with near-infrared fluorochrome, VT750-NHS, at a 3:1 fluorophore:protein molar ratio in PBS for ~2 hrs and dialyzed extensively against PBS to remove unreacted fluorophores. This reaction generated tTF-RGD carrying ~1.3 fluorophore/protein. To assess tTF-RGD accumulation in tumours, 25 ug of tTF-RGD was injected intravenously into unanaesthetized mice bearing bi-lateral MDA-MB-435 carcinoma tumours. At 24 hrs post-injection, mice were euthanized and tumours excised and weighed. Tumours were homogenized with 100 mL of SDS lysis buffer (0.1% SDS, 10 mM Tris, pH 7.6) per 30 mg of tissue, heated to 95°C for 10 minutes, and spun down at 16000 G's for 10 minutes. Supernatant fluorescence was quantified (LI-COR) and compared to a standard curve. Standards were prepared by the same procedure using tumours from uninjected animals and spiking them with known amounts of fluorophore.

Probing tTF Signalling module-mediated tumour coagulation via fibrin(ogen) deposition in tumours. To assess tTF-mediated coagulation in mice, ~1 nanomole of both fibrinogen and albumin proteins (bearing distinct NIR-fluorophores) were injected intravenously alongside varying amounts of tTF, tTF-RGD, or tTF-NGR into unanaesthetized mice bearing a flank MDA-MB-435 carcinoma tumour. At 24 hrs post-injection, mice were dissected and tumours were fluorescently imaged for the relative abundance of fibrinogen and albumin (LI-COR Odyssey Infrared Imaging System). Increases in protein tropism to tumours were analyzed by assessing mean tumour fluorescence (n=4 mice with each type of tTF tested).

Immunohistochemical analysis in tumours. For histologic analysis, frozen sections of tumours were prepared. The sections were first fixed with acetone. Rat anti-mouse CD-31 (1:50, BD PharMingen) and biotinylated mouse fibrin(ogen) antiserum (1:50, Nordic) were used for immunochemical staining of tumour tissue sections. The corresponding secondary antibodies were added and incubated for 1 hour at room temperature: AlexaFluor-594 goat anti-rat or rabbit IgG (1:1,000; Molecular Probes), streptavidin Alexa Fluor 594 (1:1000; Molecular Probes). The slides were washed three times with PBS and mounted in Vectashield Mounting Medium with DAPI. At least

three images from representative microscopic fields were analyzed for each tumour sample.

Peptide Synthesis. The three peptides used in this work: a fibrin-binding peptide (Ac-d-d-d-***G-Y-e-C-hyP-cY-G-L-C-Y-I-Q***-K-(K-Fluorescein)) (binding sequence in bold), a peptide substrate for the transglutaminase Factor XIII (G-N-***Q***-E-Q-V-S-P-L-T-L-L-K-X-C-(K-Fluorescein)) (active glutamine in bold; X=6-aminohexanoic acid linker), and a control substrate for FXIII termed "FXIIIControl" (G-N-***A***-E-Q-V-S-P-L-T-L-L-K-X-C-(K-Fluorescein)) (single amino acid substitution in bold) were synthesized via standard FMOC solid-phase peptide synthesis (MIT Biopolymers Core or Tufts University Core Facility). Products were HPLC-purified to >90% purity and characterized via mass spectrometry. Fibrin-binding peptides were cyclized by bubbling air into 10 μM aqueous peptide solutions overnight, followed by lyophilization for subsequent use.

Receiving Module NP Syntheses. Superparamagnetic, dextran-caged iron oxide nanoworms (NWs) with a longitudinal size of ~55 nm were synthesized, aminated using 20% v/v ammonium hydroxide, and derivatized with near-infrared fluorophores as described previousl (2). Fibrin-binding peptides were attached to NWs via their exogenous lysine by first reacting fluorophore-labelled NWs with the bifunctional linker NHS-PEO_5-NHS (Pierce) in phosphate buffered saline pH 7.2 (PBS) at a 5000:1 linker:NW molar ratio to prevent cross-linking. Following activation with linker, NWs were filtered using a gel filtration column (G50 media) and incubated overnight with cyclized fibrin-binding peptides at ~1000:1 peptide:NW ratio with shaking. After ~12 hrs, NWs were purified from extra peptides by repeated filtration on centrifugal membrane filters (100 kDa size cutoff, Centricon, Millipore) and finally dispersed in PBS for spectrophotometric analysis of peptide labelling. Factor XIII-substrates were attached to NWs via their exogenous cysteine similarly, but with the linker NHS-PEO_{12}-Maleimide (Pierce) in place of the bifunctional NHS-PEO_5-NHS linker. All peptide-functionalized NWs were characterized via dynamic light scattering (DLS) and intravenously injected *in vivo* to ensure all targeted NWs and control NWs exhibited similar circulation times.

Doxorubicin-loaded liposome synthesis. Hydrogenated soy sn-glycero-3-phosphocholine (HSPC), cholesterol, and 1,2-distearoyl-snglycero-3-phosphoethanolamine-N-polyethylene glycol 2000 [DSPE-PEG(2k)], 1,2-Distearoyl-sn-Glycero-3-Phosphoethanolamine-N-[Maleimide(Polyethylene Glycol 2000)] [DSPE-PEG(2k)-MAL] were purchased from Avanti Polar Lipids (Alabaster, AL). Doxorubicin was purchased from Sigma Chemical Co. (St.Louis, MO). For peptide conjugation, liposomes with maleimide groups were prepared from HSPC, cholesterol, DSPE-PEG(2k), and DSPE-PEG(2k)-MAL in the molar ratio of 75:50:3:3 by lipid film hydration and membrane (100 nm) extrusion method(3). Encapsulation of doxorubicin (DOX) into the liposomes was then carried out using the pH gradient-driven loading protocol(4). Free doxorubicin was removed by gel filtration on Sephadex G-50. After doxorubicin loading, the maleimide-terminated liposomes were reacted with thiols on peptides (FXIII and FXIIIControl) for 2 hrs and then purified by by gel filtration on Sephadex G-50. The peptide-conjugated doxorubicin liposomes were stored in PBS at 4 °C before use.

DOI: 10.1038/NMAT3049

In vitro cytotoxicity: Cytotoxicity assessments were conducted by the MIT Nanomaterials Toxicity Core using Human HeLa cervical cancer cultures (ATTC) in 96-well plates grown to ~70% confluency. Cells were incubated in quadruplicate with various dilutions of either PEG-NR or LP formulations assessed for viability after 24hrs of incubation using the fluorogenic intracellular esterase sensor Calcein acetoxymethylester (Invitrogen).

Imaging Receiving NW homing to tumours. Mixtures of NIR-fluorophore-labelled, targeted and control NWs (bearing VT750 and VT680 or VT680 and VT750, respectively) were co-adminstered intravenously in PBS (2 mg Fe/kg) to tumour-bearing nu/nu mice as described in the manuscript to provide an internal control reference for coagulation-specific NW homing. Because the half-life of targeted and untargeted FXIII-NWs (as well as LPs used in this study) were several hours and the activity of the transglutaminase FXIII has a half-life of <30min following coagulation induction(5), we chose to inject all Receiving NPs at the initiation of heating or alongside tTF Signalling modules to ensure Receivers would be present in circulation during and throughout the onset of coagulation. At 24 hrs post-NW injection, mice were sacrificed and organs were analyzed for both NIR-fluorophores (LI-COR Odyssey Infrared Imaging System). For integrated nanoparticle system characterization, mice were additionally imaged under isofluorane anaesthetic before euthanization using a whole animal fluorescence reflectance imaging system (Xenogen, IVIS Imaging System) to visualize the specificity of NW homing to tumours. Images from both organ scanning and whole animal imaging are displayed as overlaid fluorescent images from both channels (VT750=green and VT680=red). As with fibrinogen/albumin characterization earlier, all experiments were conducted with VT750-labeled targeted particles alongside VT680-labeled control particles and with VT680-labelled targeted particles alongside VT750-labeled control particles to ensure that fluorophore bias did not perturb results. For initial Receiving module characterization, levels of targeted and control NW homing were plotted by comparing the average NW fluorescence in heated tumours versus unheated tumours (n=4 mice at each temperature). For integrated network evaluation, levels were plotted by comparing the average targeted and untargeted NW fluorescence in irradiated tumours versus un-irradiated tumours (n=4 mice for all conditions). For autonomously-communicating nanosystems, NIR-fluorophore-labeled peptide-bearing NWs (bearing VT750 fluorophores) were intravenously (2 mg Fe/kg) in PBS to unanaesthetized MDA-MB-435 tumour-bearing nu/nu mice alone or alongside various tTF Signalling modules (25 μg). At 24 hrs post-NW injection, mice were sacrificed and organs were analyzed for NIR Receiver fluorescence (LI-COR Odyssey Infrared Imaging System). For intraoperative fluorescent tumour imaging, mice were anaesthesized and tumours were surgically exposed to reveal detailed tumour fluorescence (LI-COR). Levels of NW homing to tumours were plotted by comparing the average NW fluorescence in fully-excised tumours (n=4 mice at each condition). For whole animal organ distribution, tTF-RGD Signalling modules were administered intraperitoneally (25 μg) and FXIII-NWs were administered intravenously (2 mg Fe/kg) to unanaesthetized mice bearing an MDA-MB-435 tumour.

Quantifying Receiver NW accumulation in tumours via fluorescence. Quantification of NW accumulation via fluorescence was based on previously described methods. (6-7) MDA-MB-435 xenografts were established in nu/nu mice and administered with FXIII-NW as described in the manuscript. At 24 hrs post-NW administration, mice were euthanized and tumours excised and weighed. Tumours were homogenized with 100 mL of SDS lysis buffer (0.1% SDS, 10 mM Tris, pH 7.6) per 30 mg of tissue, heated to 95°C for 10 minutes, spun down at 16000 G's for 10 minutes, and re-homogenized. Homogenate fluorescence was quantified (LI-COR) and compared to a standard curve. Standards were prepared by the same procedure using tumours from uninjected animals and spiking them with known amounts of fluorophore.

Quantification of doxorubicin in tissues. MDA-MB-435 xenografts were established in nu/nu mice and administered with FXIII-LPs or FXIIIControl- LPs as described in the manuscript. At 24 hrs post-irradiation or external heating, doxorubicin in tissues was fluorescently quantified in organ homogenates. Briefly, organs were removed, weighed, incubated with 500 µl of 70% EtOH, 0.3 N HCl, and homogenized (Tissue Tearor, Biospec Products) to release doxorubicin from tissues. Following homogenization, another 1 ml of 70% EtOH, 0.3 N HCl, was added to samples and they were centrifuged. Supernatants of samples were analyzed for doxorubicin fluorescence using a fluorescence microplate reader (Molecular Devices, SpectraMax GeminiEM) and compared to standard curves.

Therapeutic assessment of communicating and control nanoparticle systems. Therapeutic studies were conducted by first intravenously administering PEG-NRs or saline into nu/nu mice bearing a single MDA-MB-435 tumour. At 72 hrs post-injection, mice were intravenously administered FXIII- LPs, FXIIIControl- LPs, or saline (in ~150 µl bolus) and broadly irradiated in the vicinity of the tumour with NIR light (810 nm, ~1 W/cm^2, 20 min). An additional cohort of mice was administered saline at 0 and 72 hrs and not exposed to NIR light in order to isolate any therapeutic efficacy of this input in isolation. Each therapeutic cohort included 7 mice, except for the unirradiated saline-only control, which had 6 mice. At regular intervals after treatment, tumours were measured and mice were weighed. Mice were sacrificed when tumours exceeded 500 mm^3.

References:

1. von Maltzahn, G. *et al.* Computationally-guided photothermal tumour therapy using long-circulating gold nanorod antennas. *Cancer Research* . 69 (9), 3892, (2009).

2. Park, J.H. *et al.* Magnetic iron oxide nanoworms for tumour targeting and imaging. *Advanced Materials* **20,** 1630-+ (2008).3. M. J. Hope, M. B. Bally, G. Webb, P. R. Cullis, *Biochimica Et Biophysica Acta* **812**, 55 (1985).

DOI: 10.1038/NMAT3049

3. L. D. Mayer, M. B. Bally, M. J. Hope, P. R. Cullis, *Biochimica Et Biophysica Acta* **816**, 294 (1985).

4. Ruf,W. et al. Phospholipid-independent and -dependent interactions required for tissue factor receptor and cofactor function. *J Biol Chem*. **266**, 2158-2166 (1991).

5. Robinson BR *et al*. Catalytic life of activated factor XIII in thrombi. Implications for fibrinolytic resistance and thrombus aging. Circulation. 2000 Sep 5;102(10):1151-7.

6. Olson, E. S. *et al.* In vivo characterization of activatable cell penetrating peptides for targeting protease activity in cancer. *Integrative Biology* **1**, 382-393 (2009).

7. Aguilera, T. A., Olson, E. S., Timmers, M. M., Jiang, T. & Tsien, R. Y. Systemic in vivo distribution of activatable cell penetrating peptides is superior to that of cell penetrating peptides. *Integrative Biology* **1**, 371-381 (2009).

Supplemental Figures:

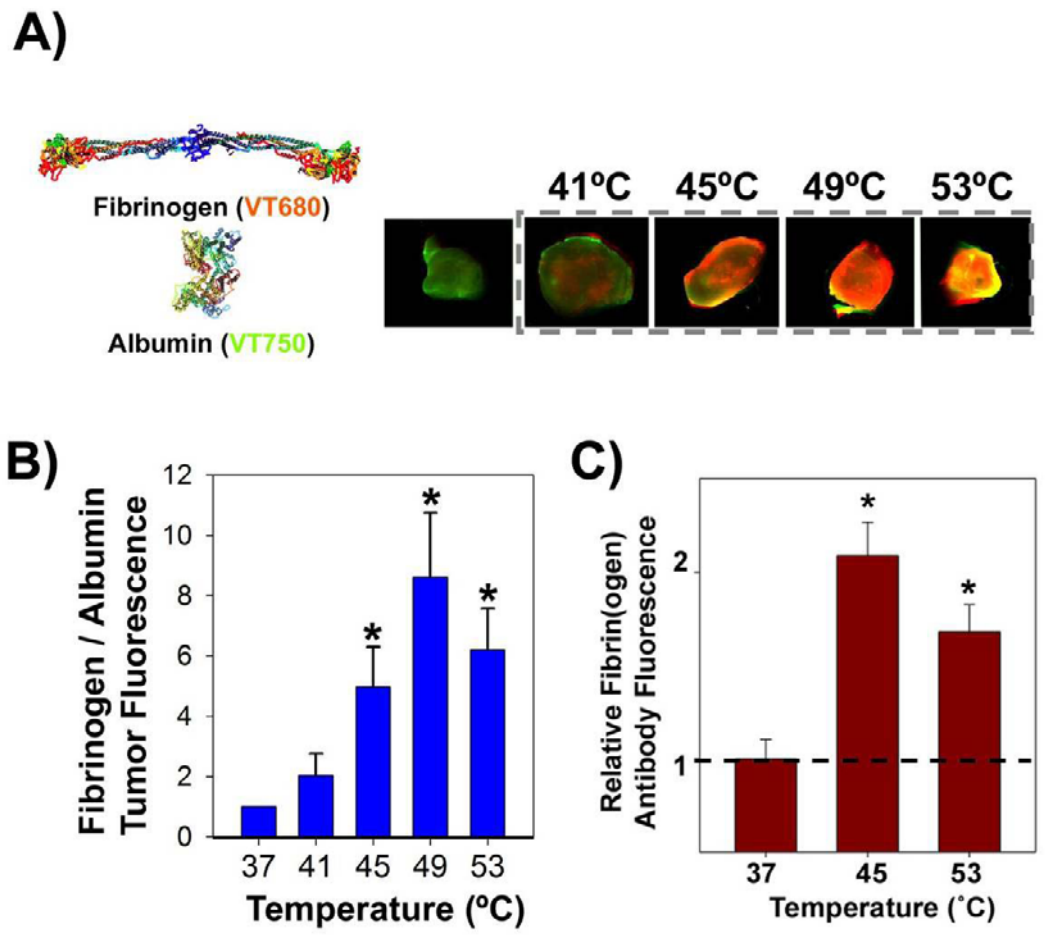

Figure S1. *Specific fibrinogen tropism to heated tumours.* A) *Probing the coagulation-dependent and –independent protein tropism to heated tumours.* Fibrinogen and albumin were labelled with unique near-infrared fluorochromes in the *opposite* channels as in Figure **2A** (VT680 and VT750, respectively) and injected in mice under identical conditions. Reversing the fluorophore labelling on fibrinogen and albumin enables quantitation of protein tropism to heated tumours independent of any potential optical or molecular fluorophore bias. At 24 hrs post-injection, mice were dissected and both tumours imaged for the relative abundance of fibrinogen (red) and albumin (green). Both heated (+ row) and unheated (- row) tumours are displayed across the temperatures tested. **B)** *Quantitation of fibrinogen:albumin fluorescence ratio across tested tumour temperatures.* Data taken under conditions of **2B** and **S1A** were utilized to quantify the relative abundance of fibrinogen and albumin in heated tumours vs unheated. At 45-53˚C, fibrinogen abundance in tumours was significantly enhanced over albumin ($p<0.05$; 1-sided t-test; 4-mice per temperature). **C)** *Quantitation of anti-fibrin(ogen) binding to sections from unheated and externally-heated tumours.* As an independent measure of fibrin(ogen) deposition in heated tumours, uninjected mice bearing bilateral

DOI: 10.1038/NMAT3049

MDA-MB-435 tumours had one tumour immersed in a temperature-controlled water bath for 20 minutes and were sacrificed 24 hrs later for histological sectioning. Fluorescent quantification showed significantly enhanced abundance of antibody binding at both 45 and 53˚C ($p<0.0001$, 1-sided t-test, 6 separate regions analyzed in each condition).

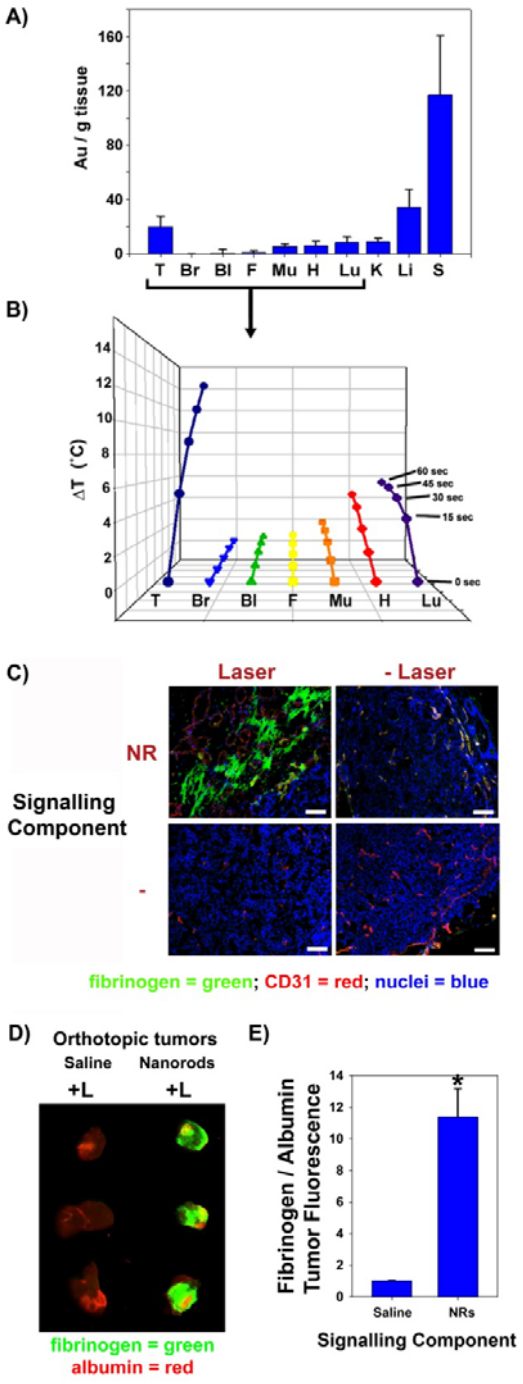

Figure S2. *Nanorod-directed fibrin(ogen) deposition in vivo.* **A)** *PEG-nanorod biodistribution and targeting to MDA-MB-435 tumours 72hrs following intravenous administration, quantified via inductively-coupled plasma mass spectrometry* (3 mice). Y-axis is micrograms Au per gram tissue. (T=tumour, Br=brain, Bl=bladder, F=fat, Mu=muscle, H=heart, Lu=lung, K=kidney, Li=liver, Sp=spleen) **B)** *Ex-vivo heating rates of dissected organs under identical irradiation conditions revealed that NR targeting confers specificity to photothermal tumour heating.* Mice bearing a single

DOI: 10.1038/NMAT3049

MDA-MB-435 tumour were injected with PEG-NR Signalling modules and, 72 hrs after injection, were dissected for comparison of photothermal organ heating rates. **C)** *Histopathological analysis of NR-directed fibrinogen deposition in tumours.* Mice bearing bilateral MDA-MB-435 tumours were injected with PEG-NRs (10 mg Au/kg) or saline and, 72 hrs later, injected with fluorescently-labeled fibrinogen (VT750) and broadly irradiated on their right side (~1 W/cm^2, 810 nm, 20 min). At 24 hrs post-injection, mice were sacrificed and tumours isolated for histological analysis of fibrinogen distribution (Red=CD31 antibody stain, Blue= DAPI nuclear stain, Green=fibrinogen distribution) (Scale bars=100 μm). **D)** *Probing the photothermal induction of coagulation in orthotopic MDA-MB-435 tumours implanted deep in the mammary fat pad.* Mice bearing a single MDA-MB-435 tumour were injected with PEG-NRs (10 mg Au/kg) or saline and, 72 hrs later, injected with fluorescently-labeled fibrinogen (VT750) and albumin (VT680) and broadly irradiated with extracorporeal light (~1.5 W/cm^2, 810 nm, 20 min). At 24 hrs post-injection, mice were sacrificed and tumours isolated for fluorescent imaging of relative fibrin(ogen) (*green)* and albumin *(red)* accumulation. **E)** *Quantitation of fibrinogen:albumin fluorescence ratio across tested tumour temperatures.* Data taken under conditions of **D)** were utilized to quantify the relative abundance of fibrinogen and albumin in tumours from mice injected with saline and NRs.

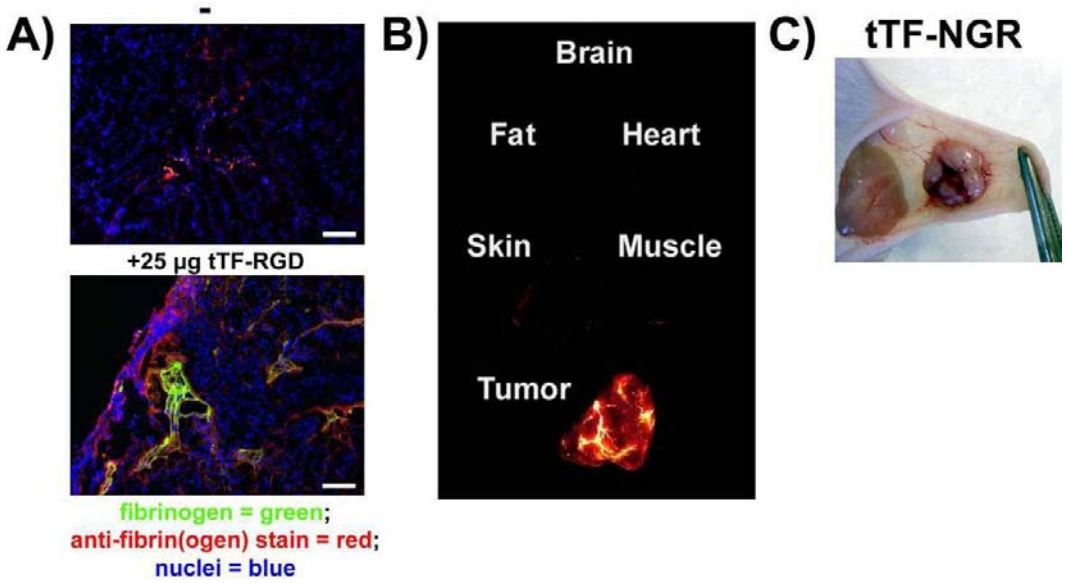

Figure S3. *tTF-RGD and tTF-NGR Signalling module characterization* **A)** *Anti-fibrin(ogen) antibody stain reveals little fibrin(ogen) in tumours of mice injected with saline (*top*) and fluorescent fibrin(ogen) and abundant fibrin(ogen) in tumours of tTF-RGD-injected mice that co-localizes with injected fibrin(ogen) fluorescence* (bottom)(Red = Anti-fibrinogen stain; Green = injected fibrinogen fluorescence; Blue = nuclear stain), top = VT750-labeled fibrinogen without tTF-RGD injection; bottom = VT750-labeled fibrinogen with tTF-RGD injection (1 mg tTF-RGD/kg) (Scale bars = 100 μm). **B)** *Macroscopic distribution of fluorescent fibrinogen in tTF-RGD Signalling module –injected mice.* Organs were imaged at 24 hrs following intravenous co-injection of fluorescent fibrinogen with tTF-RGD Signalling module (1 mg tTF-RGD/kg) (~1 nmole fibrinogen; VT750 fluorophore). *Intraoperative images at 24-hrs post-tTF-NGR Signalling module (which binds CD13/aminopeptidase N receptors associated with tumour angiogenesis) injection highlighting modularity of tTF Signalling modules. Nu/nu* mice bearing a single MDA-MB-435 tumour were intravenously injected with tTF-NGR (1 mg of tTF-NGR/kg) and dissected 24 hrs later. Administration of both tTF-NGR or tTF-RGD led to the macroscopic appearance of tumoural hemorrhage and RBC stasis, while saline-injected mice harbored ivory-hued tumours (see Figure 2 of manuscript for tTF-RGD and saline).

DOI: 10.1038/NMAT3049

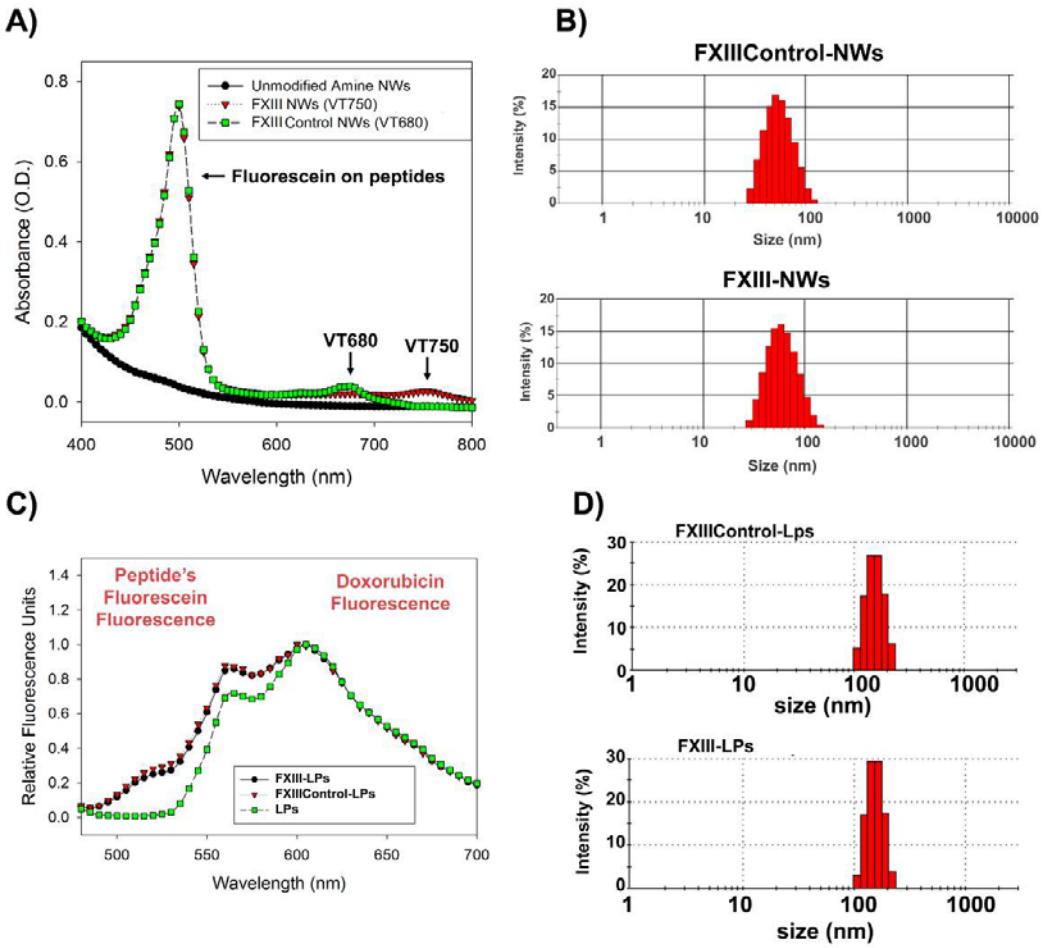

Figure S4. *Spectrophotometric, fluorescent, and size characterization of Receiving modules.* **A)** Spectrophotometric characterization of NW Receiving module functionalization. Aminated NWs were conjugated with NHS-activated NIR fluorochromes (VT680 or VT750) to allow fluorescent imaging and subsequently linked to thiol-containing FXIII-substrate peptides or FXIIIControl-peptides. The spectra NWs were utilized to quantify the number of peptides and NIR-fluorochromes per particle (~600 FXIII- or FXIIIControl-peptides/NW and ~12-15 fluorochromes/NW, respectively). Conjugation conditions were optimized to produce populations with approximately equal numbers of peptides in the FXIII-NWs and FXIIIControl-NWs. **B)** Dynamic light scattering characterization of FXIIIControl-NW and FXIII-NW Receiving modules. After peptide functionalization with NIR-fluorochromes and peptides, samples were analyzed via DLS to probe the hydrodynamic size of each conjugate. **C)** Fluorescent characterization of FXIIIControl-LPs and FXIII-LPs. The fluorescence emission spectra of Fluorescein-conataining FXIII- and FXIIIControl-peptides was utilized to ensure similar surface density on LP conjugates (excitation: 444 nm; cutoff: 455 nm; emission 480 nm-700 nm). **D)** Dynamic light scattering characterization of FXIII-LP and FXIIIControl-LP Receiving modules. After peptide functionalization, LP Receiving modules were analyzed via DLS to probe the hydrodynamic size of each conjugate.

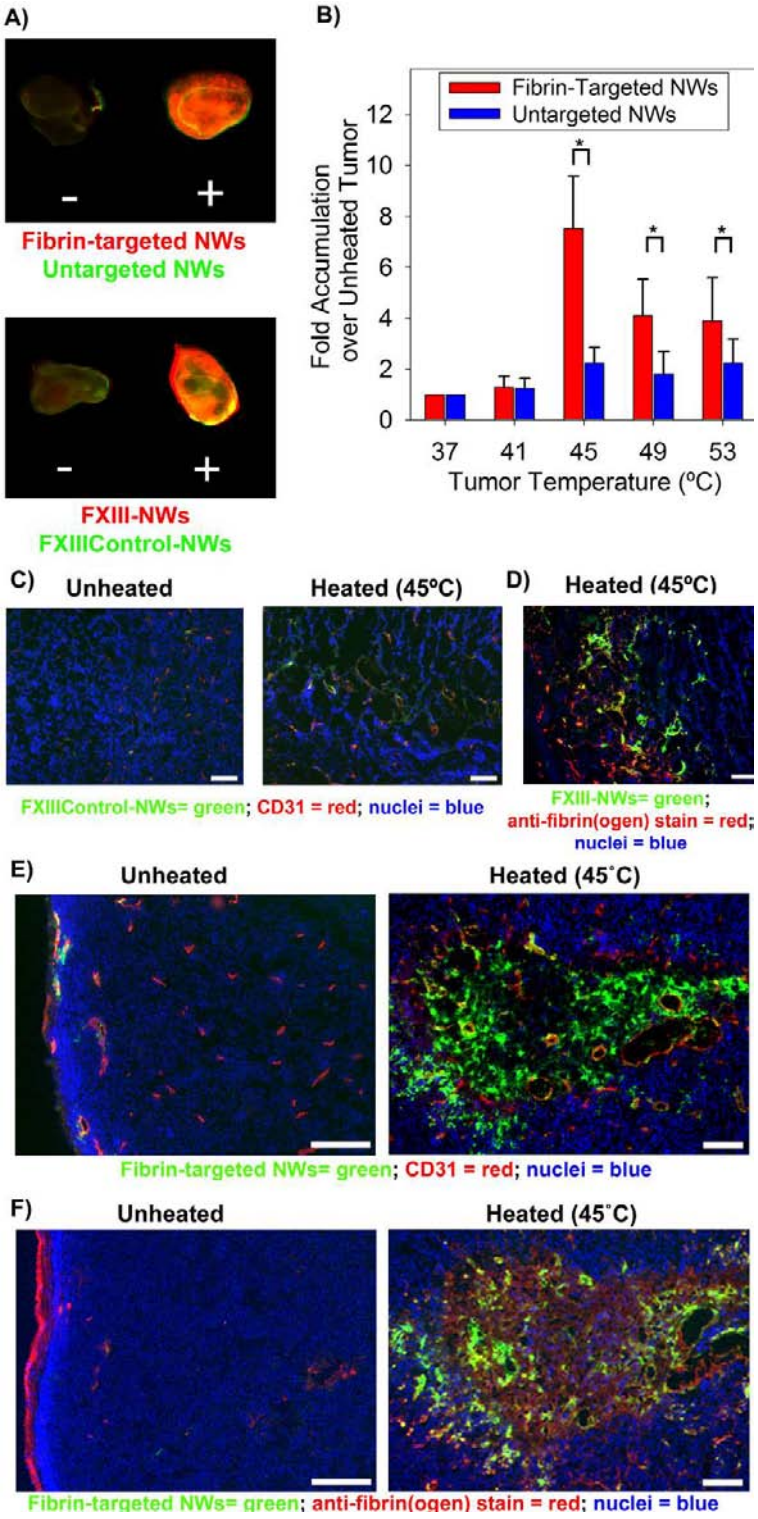

Figure S5. *NW Receiver Characterization.* **A)** *Fluoresence reflectance imaging of Receiving module homing to externally-heated tumours.* Mixtures of targeted (red) and untargeted (green) NWs (labelled with the opposite orientation of NIR-fluorochromes

DOI: 10.1038/NMAT3049

used in Figure **3C** to control against potential optical or molecular fluorochrome bias to Receiving module detection in heated vs unheated tumours**)** VT680 and VT750, respectively, were intravenously injected into mice bearing bilateral MDA-MB-435 tumours. Immediately following injection, one tumour was submerged in a temperature-controlled water bath for 20 min and mice were dissected at 24 hrs for fluorescent organ imaging. Overlaid fluorescence images are shown for targeted (green) and untargeted (red) Receiving module accumulation in both heated ("+", 45ºC heating) and naïve ("-") tumours are shown from the same mouse. **B)** *Fluorescent quantification of fibrin-binding and untargeted-NW Receiving module homing to heated over unheated tumours.* The fold enhancement of NW targeting is plotted across the range of temperatures tested (n=4 mice in each set, $p<0.05$ for the difference between fibrin-binding-NWs and untargeted-NWs at 45ºC, 49ºC, and 53ºC, respectively). **C)** *Histopathological analysis of FXIIIControl- NWs.* Mice bearing bilateral MDA-MB-435 tumours were injected with control-substrate NWs and one tumour was heated to 45ºC for 20 min. At 24 hrs post-injection, mice were sacrificed and tumours were analyzed for NW distribution in histology using the same exposure conditions for NW imaging as Figure S8, S10, and Figure 3D. (Red=CD31 antibody stain, Blue= DAPI nuclear stain, Green=FXIIIControl- NW distribution) (Scale bar=100 μm) **D)** *Histopathological analysis of FXIII-substrate localization to areas of anti-fibrin(ogen) staining.* Mice bearing bilateral MDA-MB-435 tumours were injected with FXIII-NWs and one tumour was heated to 45ºC for 20 min. At 24 hrs post-injection, mice were sacrificed and tumours were analyzed for NW distribution in histology using the same exposure conditions for NW imaging as Figure S8, S9, and Figure 3D. (Red=anti-fibrin(ogen) antibody stain, Blue= DAPI nuclear stain, Green=FXIII- NW distribution) (Scale bar=100 μm) **E)** *Histopathological analysis of FXIII-substrate localization to areas of anti-fibrin(ogen) staining.* Mice bearing bilateral MDA-MB-435 tumours were injected with FXIII-NWs and one tumour was heated to 45ºC for 20 min. At 24 hrs post-injection, mice were sacrificed and tumours were analyzed for NW distribution in histology using the same exposure conditions for NW imaging as Figure S8, S9, and Figure 3D. (Red=anti-fibrin(ogen) antibody stain, Blue= DAPI nuclear stain, Green=FXIII- NW distribution) (Scale bar=100 μm) **F)** *Distribution of fibrin-targeted NWs in unheated tumours.* (Red=CD31 antibody stain, Blue= DAPI nuclear stain, Green=fibrin-targeted NW distribution) (Scale bar=100 μm) **G)** *Distribution of fibrin-targeted NWs in unheated tumours.* (Red=CD31 antibody stain, Blue= DAPI nuclear stain, Green=fibrin-targeted NW distribution) (Scale bar=100 μm) **H)** *Co-localization of fibrin-targeted NWs with anti-fibrin(ogen) antibody staining in heated tumours.* (Red=anti-fibrinogen antibody stain, Blue= DAPI nuclear stain, Green=fibrin-targeted NW distribution) (Scale bar=100 μm) **I)** *Co-localization of fibrin-targeted NWs with anti-fibrin(ogen) antibody staining in heated tumours.* (Red=anti-fibrinogen antibody stain, Blue= DAPI nuclear stain, Green=fibrin-targeted NW distribution) (Scale bar=100 μm)

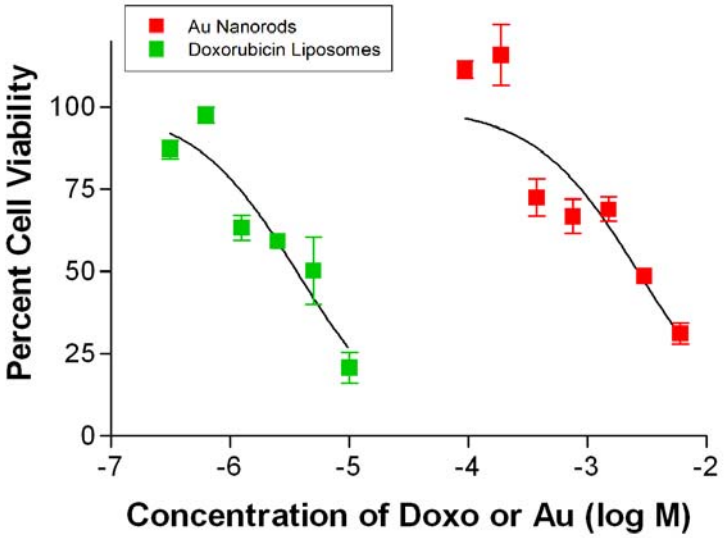

Figure S6. *Cytotoxicity experiments to assess intrinsic toxicity of Au nanorods and doxorobicin-loaded liposomes.* Cytotoxicity assessments were conducted using Human HeLa cervical cancer cultures (ATTC) in 96well plates grown to ~70% confluency. Cells were incubated with various dilutions of either PEG-NR or LP formulations assessed for viability after 24hrs of incubation using the fluorogenic intracellular esterase sensor Calcein acetoxymethylester (each point represents the average of 4 wells in a 96-well plate).

DOI: 10.1038/NMAT3049

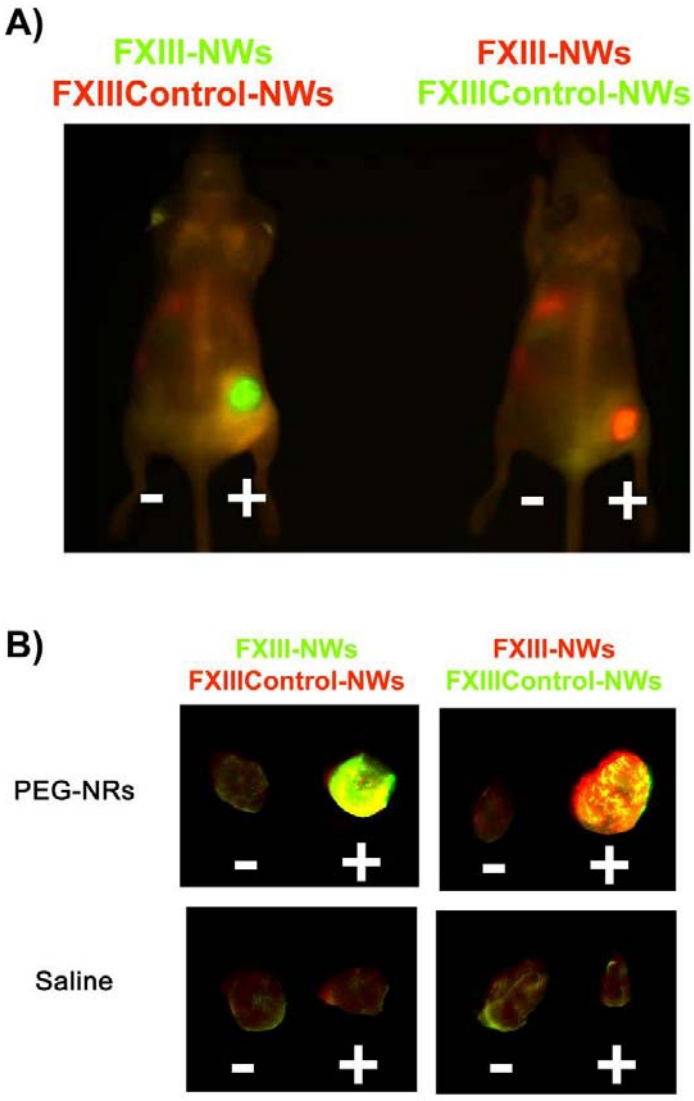

Figure S7. *Integrated communicating nanoparticles from Figure 4D, but with inverted fluorophore-targeting ligand relationships to control against bias and ex-vivo imaging of excised tumours.* A) Simultaneous near-infrared imaging of co-injected: VT750-labeled, FXIII- NWs (green, left mouse) and VT680-labeled, FXIIIControl- NWs (red, left mouse); or VT680-labeled, FXIII-NW (red, right mouse) and VT750-labeled, FXIIIControl- NWs (green, right mouse). Inversion of fluorochrome-NW relationships prevents optical or molecular bias from fluorophores in homing visualization. + indicates broad laser irradiation (810 nm, 0.75 W/cm^2, 20 min). B) Imaging of NW homing in excised tumours from experiments in Figures 4D and S12A. Each box was imaged using the same acquisition parameters for both VT750 (green) and VT680 (red) and contains the left and right tumours from MDA-MB-435-bearing mice.

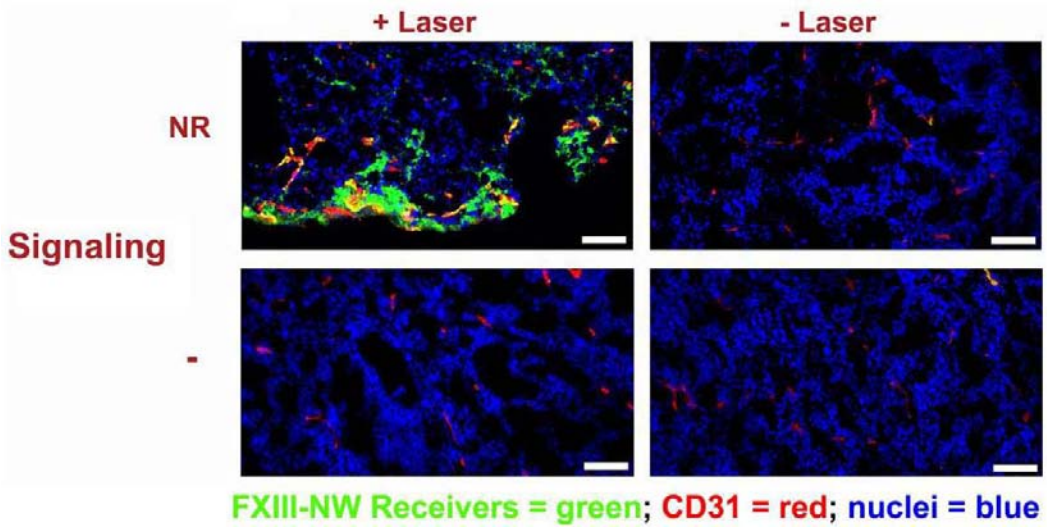

Figure S8. *Histopathological analysis of FXIII-NWs with integrated and disconnected NP communication systems.* Histopathological sections from the integrated NP Signalling experiments in Figures 4C, 4D, 4E and S12. At 24 hrs post-NW injection, mice were sacrificed and tumours were analyzed for FXIII-NW distribution in histology. (Red=CD31 antibody stain, Blue= DAPI nuclear stain, Green=FXIII-NW distribution). (Scale bars = 100 μm)

DOI: 10.1038/NMAT3049

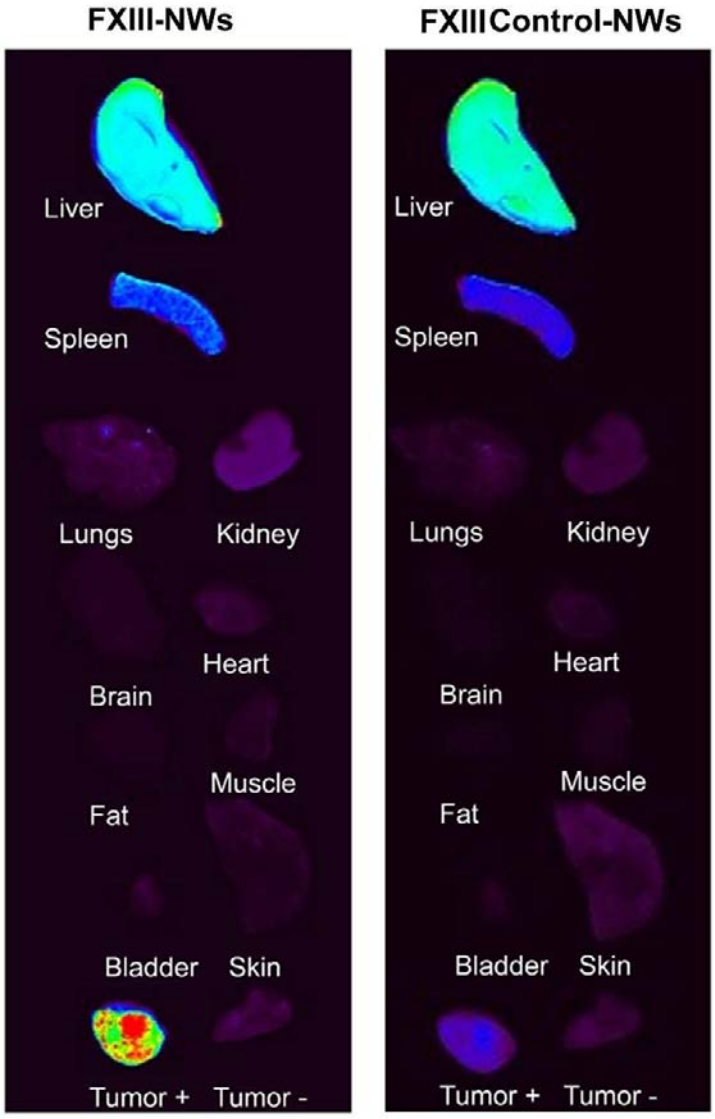

Figure S9. *Function of NP communication to human cervical xenograft tumours.* Athymic (*nu/nu*) mice bearing bilateral Hela human cervical cancer tumours were injected with PEG-NRs and, 72 hrs later, a mixture of FXIII- NWs and FXIIIControl-NWs, labelled with unique NIR-fluorophores, as described for MDA-MB-435 tumour-bearing mice in Figure 4. Immediately following injection of NW mixtures, the right flanks of mice were broadly irradiated with a diode laser source. At 24 hrs post-injection, the homing of FXIII-NWs and FXIIIControl-NWs was visualized using NIR fluorescent organ imaging. ("Tumour +" indicates the irradiated tumour; "Tumour –" was not exposed to diode irradiation)

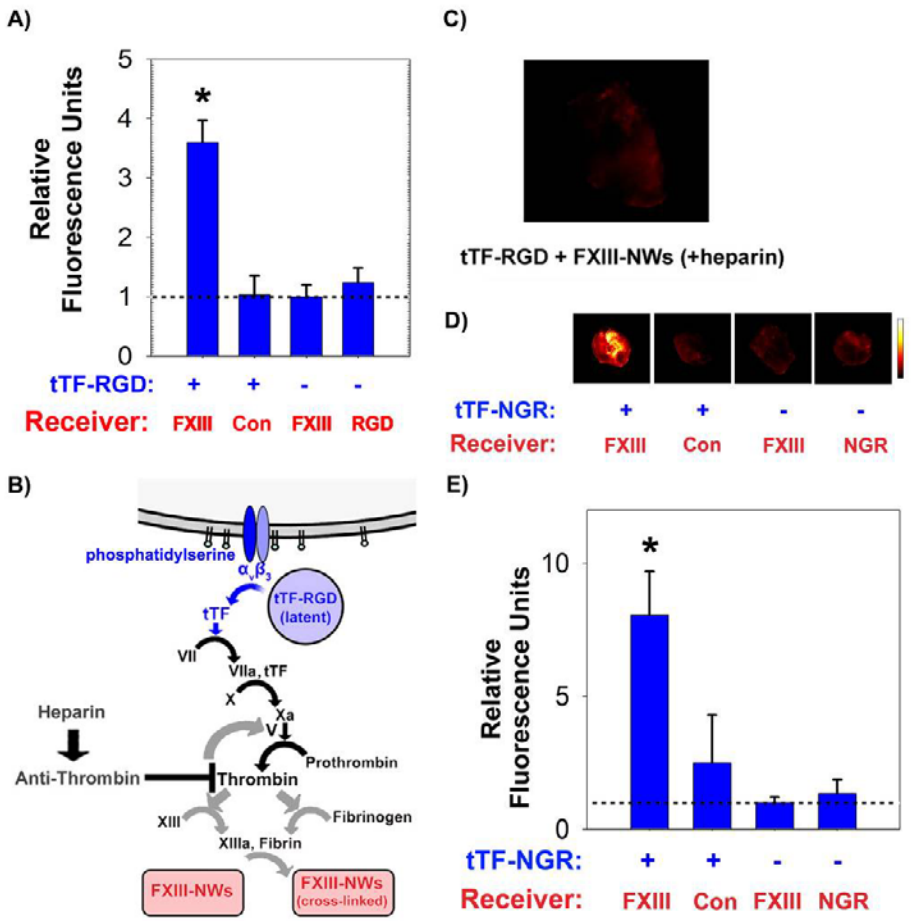

Figure S10. *Characterization of autonomously-communicating nanosystems.* **A)** *Fluorescent quantitation of NW homing in integrated Signalling networks and controls from mice in experiment from Figure 4H* (Con=FXIIIControl-NWs) (*p<0.05 versus all other sets, n=4 mice for each set) **B)** *Heparin-mediated disruption of Signalling network communication*. Schematic of heparin's disruption of communication in hybrid Signalling ne tworks. **C)** *Nu/nu* mice bearing a single MDA-MB-435 tumour were intravenously injected with integrated Signalling networks (tTF-RGD + FXIII-NWs; 1 mg/kg tTF-RGD; 1.5 mg Fe/kg) alongside heparin to prohibit thrombin activation (intravenous bolus of 800 units/kg + intraperitoneal bolus of 500 units/kg 30 minutes later). At 24 hrs post-injection, mice were sacrificed and tumours were surgically removed for fluorescent imaging of NW localization to tumours. Tumours on heparin-injected mice lack characteristic vascular pattern of communication between tTF Signalling modules and FXIII-NW Receivers. **D)** *Modularity of autonomously-communicating nanosystems.* tTF-NGR Signalling modules (which bind CD13/aminopeptidase N receptors associated with tumour angiogenesis) were substituted for tTF-RGD Signalling modules to explore the composability of autonomously-communicating systems. *Nu/nu* mice bearing a single MDA-MB-435 tumour were intravenously injected with communicating (tTF-NGR + FXIII-NWs) or control (tTF-NGR + FXIIIControl-NWs) nanosystems, FXIII-NWs alone, or NWs

DOI: 10.1038/NMAT3049

targeted by the peptide used to direct tTF-NGR Signalling module tumour homing (1 mg/kg tTF-NGR; 1.5 mg Fe/kg). At 24 hrs post-injection, mice were sacrificed and tumours were surgically removed for fluorescent imaging of NW localization to tumours (Con=FXIIIControl-NWs). **E)** Quantification of average fluorescence from tumour cohorts above (n = 3 or 4 mice in each set; error bar indicates standard deviation of data; Student's one-tailed t-test: p=0.006, 0.0015, and 0.001 for tTF-NGR + FXIII-NWs vs. tTF-NGR + FXIIIControl-NWs, FXIII-NWs, and NGR-NWs respectively) (Con=FXIIIControl-NWs).

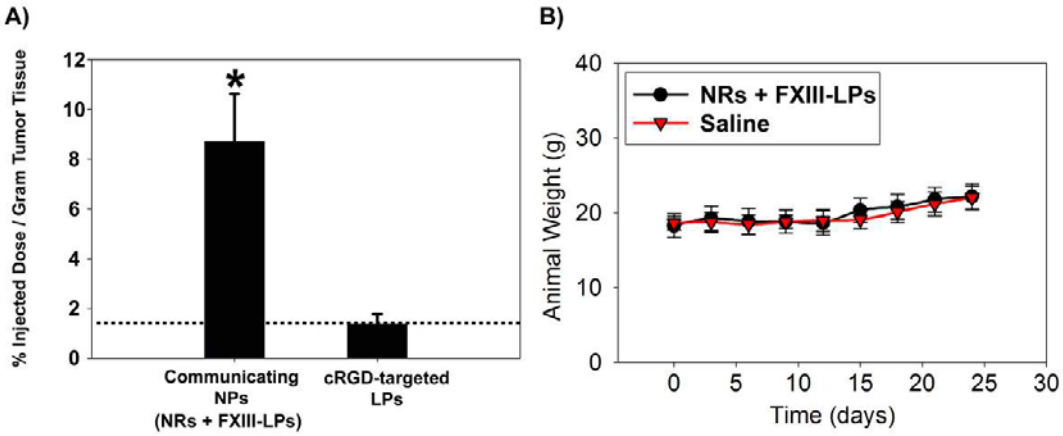

Figure S11. *Therapeutic communicating nanoparticles* **A)** *Comparison between doxorubicin delivery to tumours with communicating LPs and an optimized formulation of cRGD-LPs designed to target the endogenous tumour markers αvβ3 via cyclic RGD peptides.* Communicating NPs (NRs + FXIII-LPs) deliver over 6-fold higher doses of doxorubicin per gram of tumour tissue. **B)** *Animal weights for mice treated with therapeutic nanoparticle systems compared with those administered saline only.*

DOI: 10.1038/NMAT3049

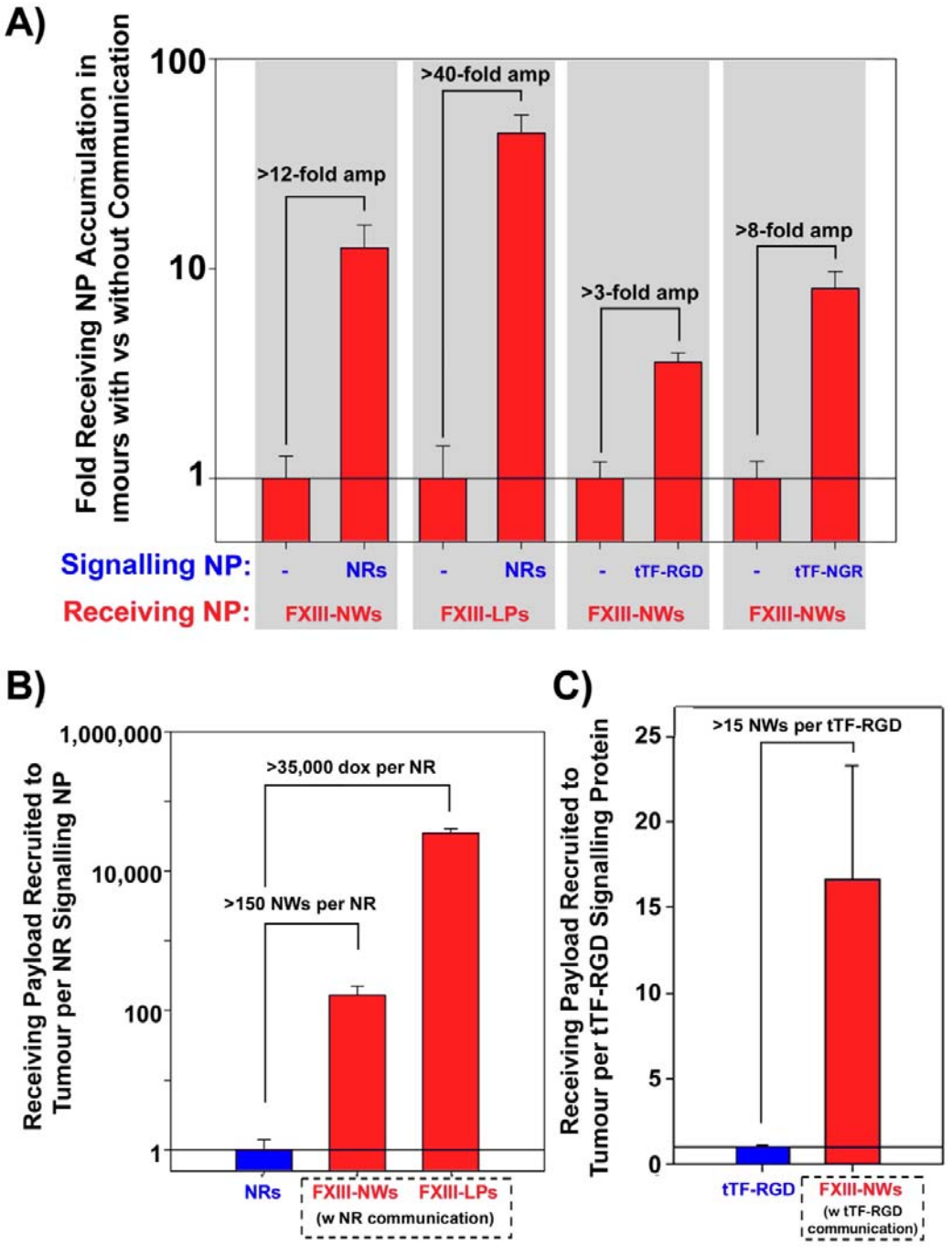

Figure 12. *Probing the ability of communication to amplify Receiving Module localization to tumours.* **A)** *Summary of Receiving Module targeting with vs without communication (tested via exclusion of Signalling NPs).* Data from Figures 4E, 5B, S10A, and S10D were compiled to provide a consolidated comparison of Receiving module targeting to tumours with vs without communication. **B)** *Assessing the amplification achieved during Signalling-to-Receiving communication using NR*

Signalling modules. In order to understand the degree to which NR Signalling modules could recruit multiple Receiving payloads, both diagnostic (iron oxide nanocrystals) and therapeutic (doxorubicin drugs), to tumours, the concentrations of: NR Signalling Modules in tumours (10mg/kg injected dose); FXIII-NWs Receivers in tumours (2 mg/kg, with communication from NRs); and the concentration of doxorubicin (2mg/kg, encapsulated within FXIII-LP Receivers with communication from NRs) were quantified and plotted to display their relative abundance in tumours. In the two systems, respectively, each tumour-localized NR Signalling module was able to recruit >150 NWs or >35,000 doxorubicin molecules from circulation. **C)** *Assessing the amplification achieved during Signalling-to-Receiving module communication using tTF-RGD Signalling modules*. In order to understand the degree to which tTF-RGD Signalling modules could recruit multiple diagnostic (iron oxide nanocrystals) Receiving payloads to tumours, the concentrations of: tTF-RGD Signalling Modules in tumours (25 ug of tTF-RGD per mouse) and FXIII-NW Receivers in tumours (2 mg/kg, with communication from tTF-RGD) were quantified and plotted to display their relative abundance in tumours. In this system, each tumour-localized tTF-RGD was able to recruit >15 NW Receivers from circulation.